Mon. Not. R. Astron. Soc. **000**, 1–12 (2009) Printed 29 November 2009 (MN LaTeX style file v2.2)

arXiv:0911.5476v1 [astro-ph.SR] 29 Nov 2009

Dynamo Processes in the T Tauri star V410 Tau*

M.B. Skelly[1]†, J.-F. Donati[1], J. Bouvier[2], K.N. Grankin[3], Y.C. Unruh[4], S.A. Artemenko[3], P.Petrov[3]
[1] *Observatoire Midi-Pyrenees, LATT, 14 avenue Edouard Belin, Toulouse, 31400, France*
[2] *Laboratoire d'Astrophysique de Grenoble, Observatoire de Grenoble, BP 53, 38041, Grenoble, France*
[3] *Crimean Astrophysical Observatory, Nauchny, Crimea 334413, Ukraine*
[4] *Astrophysics Group, Imperial College of Science, Technology and Medicine, London SW7 2AZ*

11th November 2009

ABSTRACT

We present new brightness and magnetic images of the weak-line T Tauri star V410 Tau, made using data from the NARVAL spectropolarimeter at Télescope Bernard Lyot (TBL). The brightness image shows a large polar spot and significant spot coverage at lower latitudes. The magnetic maps show a field that is predominantly dipolar and non-axisymmetric with a strong azimuthal component. The field is 50% poloidal and 50% toroidal, and there is very little differential rotation apparent from the magnetic images.

A photometric monitoring campaign on this star has previously revealed V–band variability of up to 0.6 magnitudes but in 2009 the lightcurve is much flatter. The Doppler image presented here is consistent with this low variability. Calculating the flux predicted by the mapped spot distribution gives an peak-to-peak variability of 0.04 magnitudes. The reduction in the amplitude of the lightcurve, compared with previous observations, appears to be related to a change in the distribution of the spots, rather than the number or area.

This paper is the first from a Zeeman-Doppler imaging campaign being carried out on V410 Tau between 2009–2012 at TBL. During this time it is expected that the lightcurve will return to a high amplitude state, allowing us to ascertain whether the photometric changes are accompanied by a change in the magnetic field topology.

Key words: stars: formation – stars: pre-main sequence – stars: rotation – stars: magnetic fields – stars: individual: V410 Tau

1 INTRODUCTION

T Tauri stars (TTS) are pre-main sequence late-type stars. As they contract towards the main sequence the increasing density in their interiors will lead to the development of a radiative core, if the star is sufficiently massive. A point of uncertainty concerns the evolution of their dynamos. In fully convective stars, or stars with small radiative cores, we expect the dynamo to look fundamentally different to that of the Sun. We presume that the solar dynamo is concentrated in the boundary between the convective and radiative layers, known as the tachocline. As the radiative core in the young star grows the dynamo should change from being distributed throughout the convective zone to being confined to the tachocline. Observations of young stars with a range of ages, masses and rotation rates will help to illuminate this process.

V410 Tau is one of the most well-observed TTS. It is a weak-line T Tauri star (wTTS) which has already dissipated its disk, hence it does not display signatures of accretion characteristic of classical TTS (cTTS). It has a $v \sin i$ of 74 ± 3 km s^{-1} and a period of 1.872 days (Stelzer et al. 2003), and is therefore an example of the young, rapidly rotating stars which are characterised by strong, large scale magnetic fields. Other, more evolved, examples include the 10 Myr old TWA 6 (Skelly et al. 2008), Speedy Mic (20 Myr, Barnes et al. 2001; Barnes 2005; Dunstone et al. 2006) and AB Dor (50 Myr, Collier Cameron & Donati 2002; Donati et al. 2003a; Jeffers et al. 2007).

The strong fields in these stars have either been directly measured using Zeeman-Doppler imaging (ZDI, Semel 1989; Donati et al. 1997, 2006), or their presence indicated indirectly e.g. by the large spot coverage on the surface. In the case of V410 Tau this field has revealed itself in the presence of cool spots covering a large fraction of the photosphere. In fact, V410 Tau has exhibited one of the highest optical variabilities observed on a young star, with ΔV reaching 0.6 magnitudes (Stelzer et al. 2003; Grankin et al. 2008).

---

* Based on observations obtained at the Télescope Bernard Lyot (TBL), operated by CNRS/INSU.
† E-mail: mskelly@ast.obs-mip.fr

V410 Tau is the target of an ongoing photometric monitoring campaign which began in 1981 (Vrba et al. 1988; Herbst 1989; Petrov et al. 1994; Grankin et al. 2008). For most of this time the lightcurve has been smooth, repeating, with a clearly defined period and an amplitude between 0.2 and 0.6 magnitudes.

Two significant decreases in the amplitude of the lightcurve, where ΔV fell below 0.2, have been observed during this campaign. The first of these was between 1981–1983 and the second began in 2005, reaching a minimum in 2007. Additional observations of V410 Tau dating from 1905–1987 are available on photographic plates in the archives of the Sternberg Astronomy Institute. Sokoloff et al. (2008) have digitised this data and used it to investigate the variability over a longer period of time. This revealed a third decrease in lightcurve amplitude between 1963–1970, this time in the *B*–band.

These changes in the lightcurves suggest a rearrangement of the cool spots. Given that starspots are a magnetic phenomenon such a change is likely to be caused by a change in the magnetic topology. The fact that this change has been observed three times with intervals of approximately 20 years may be evidence of a stellar cycle, similar to the 22-year solar cycle. The existence of magnetic cycles in active stars has been extensively investigated through changes in their starspot coverage (see, e.g., Berdyugina 2005; Strassmeier 2009, and references therein). Possible short-period cycles (of between 5–7 years) have been found on V410 Tau by Stelzer et al. (2003) and Oláh et al. (2009), using photometric data spanning several decades.

Doppler imaging (Vogt et al. 1987; Strassmeier 2002) can provide more detail on the changes in spot distribution. Maps of the spot distribution on V410 Tau have been made by Joncour et al. (1994); Hatzes (1995a) and Rice & Strassmeier (1996). The images have shown decentred polar spots and low latitude spots. Often the lower latitudes features are found to be confined within particular longitude ranges (e.g. Rice & Strassmeier 1996).

The flattening of the lightcurve suggests that a change in the distribution or number of photospheric spots has occurred, i.e., either there are fewer spots than previously or there is a more even longitudinal distribution of spots. Grankin et al. (2008) found a stronger correlation between the non-uniformity of the spot distribution and the amplitude of the lightcurve than the total spot area. This suggests that the reduction in lightcurve amplitude is related to a rearrangement in the spot distribution, rather than a change in the number or area of the spots.

To date, no magnetic images of V410 Tau have been published. This has motivated a long–term campaign, being carried out at Télescope Bernard Lyot (TBL), which aims to produce several spot and magnetic maps of V410 Tau between 2009–2012. We expect that during this time the lightcurve will return to the state observed between 1988–2004. In this paper we present the first set of images. Sec. 2 discusses the evolutionary status of V410 Tau. Sec. 3 describes the observations and data reduction; in Sec. 4 we describe the image production and present the brightness and magnetic images, and a new measurement of the differential rotation. Sec. 5 is a discussion of the implication of the results for the dynamo theory in pre-main sequence stars.

2 PHYSICAL PARAMETERS OF V410 TAU

The evolutionary state of V410 Tau is somewhat uncertain. The $v \sin i$ and period quoted above indicate a minimum stellar radius of 2.8 $R_\odot$. Widely varying effective temperatures have been reported in the literature, including 4700 K (e.g., Bertout et al. 2007) and 4060 K (e.g., Sestito et al. 2008). In this work we adopt a temperature of 4500 ± 100 K, in better agreement with the B - V value of 1.16 from Grankin et al. (2008) and the temperature calibrations of Bessell et al. (1998).

With this temperature and minimum radius we can estimate the minimum luminosity to be 3.4 $L_\odot$. Wichmann et al. (1998) and Bertout et al. (1999) give a range of distances of 116–157 pc, based on *Hipparcos* (ESA 1997) measurements. Assuming the lowest observed V magnitude (10.52) in Grankin (1999) is the unspotted V magnitude, and a distance of 157 pc gives a luminosity of 2.4 $L_\odot$ (if $A_v = 0$), well below the minimum luminosity calculated above.

The discrepancy suggests that even when we observe the star at its brightest, it still has significant spot coverage. In other words, the true "unspotted" magnitude is brighter than 10.52. This possibility was explored in Grankin (1999), who calculated an absolute unspotted V mag of 10.236, 0.28 mag brighter than their minimum observed magnitude. This would mean that the star has an even distribution of small spots across its surface at all times that are not detected by Doppler imaging, as they are smaller than the resolution limit.

Using an inclination of $70 \pm 10°$ (obtained in the imaging process, see Sec. 4.2) gives a radius of 3.0 $R_\odot$, and with a temperature of 4500 K indicates (using the models of Siess et al. 2000) that V410 Tau has a mass of $1.4 \pm 0.2\ M_\odot$ and an age of 1.2 ± 0.3 Myr. This is much younger than previously indicated, e.g. in Bertout et al. (2007), where an age of 6 Myr was given for V410 Tau. The parameters given in Bertout et al. (2007) are consistent with a radius of 1.8 $R_\odot$, which is incompatible with the $v \sin i$ and period.

These parameters indicate (again using the models of Siess et al. 2000) that the radiative core has a radius of $0.1R_*$. The uncertainties in the temperature and inclination allow the radiative core to have a radius between $0.0 - 0.28R_*$, meaning that the star could be fully convective.

Some interesting questions arise when we consider the possibility of a stellar cycle, particularly as we expect that a star which is fully convective or has a small radiative core has close to 'solid body' rotation (Barnes et al. 2005).

Differential rotation is crucial to the solar magnetic cycle, as it allows the development of toroidal field from poloidal field by shearing the field lines (Parker 1955). This may not rule out the possibility of cyclical dynamos existing without differential rotation. For example, Rüdiger et al. (2003) modelled α^2 dynamos and found that oscillatory solutions appear in turbulent spherical shells in exceptional cases. However, they conclude that cyclical activity is almost always indicative of differential rotation.

Previous attempts to detect differential rotation on V410 Tau have found it to be very small. Rice & Strassmeier (1996) obtained a value for the differential rotation parameter $\Delta\Omega$ of 0.003, around 1/20 of the solar value. If the star does indeed have a cycle it appears this must arise with very little differential rotation.

3 OBSERVATIONS AND DATA ANALYSIS

Spectroscopic observations of V410 Tau were made at the 2-m Télescope Bernard Lyot (TBL) on Pic du Midi in the French Pyrénées between 02–17 January 2009. During this time, 40 spectra were taken using the spectropolarimeter NARVAL (the twin of ESPADONS on the Canada France Hawaii Telescope), with four sub-exposures taken in different polarimeter configurations each time. This allows spurious polarisation signals to be removed to first order (Donati et al. 1997). The integration times (for the individual sub-exposures) were 600s, except for the observations taken on 10 January 2009 which had integration times of 800s.

The full wavelength range of the spectra was $370-1000$ nm, taken with a spectral resolution of 60000 and a velocity pixel step of 2.6 km s^{-1}, reduced to approximately 1.8 km s^{-1} as the spectrograph slit was tilted with respect to the CCD pixels. The full observing log is given in Tab. 1. In the table the rotational phase of V410 Tau at each observation is given with respect to the ephemeris,

$$\mathrm{JD(Hel.)} = 2454832.58033 + 1.87197\mathrm{R}, \tag{1}$$

where R is an integer number of rotations. This uses the same period and zero phase as Stelzer et al. (2003). The resulting phase coverage is good, covering around 75% of the surface and there is close phase correspondence between several of the observations providing a good opportunity to measure differential rotation (see Sec. 4.4).

The data was reduced using Libre ESpRIT, a dedicated pipeline for the reduction of spectropolarimetric data taken at TBL and CFHT. This package automatically extracts the unpolarised and polarised spectra, as described in Donati et al. (1997). To improve the effective signal-to-noise ratio of the data least–squares deconvolution (LSD, Donati et al. 1997) was applied to each spectrum, i.e., a line list was deconvolved from each spectrum, revealing in each case the underlying rotationally broadened profile. Mean intensity (Stokes I) and circularly polarised (Stokes V) profiles were produced in this way. The line list was created using an atlas9 model atmosphere (Kurucz 1993), using a spectral type of K5, and contained just under 9000 absorption lines in total. The Stokes I profiles show distortions characteristic of photospheric spots and Zeeman signatures were detected in most spectra, with a typical peak-to-peak amplitude of 0.2%, i.e. 10 times the noise level. Example Stokes I and V profiles are shown in Fig. 1.

We used the I and V profiles to directly calculate the magnetic field along the line-of-sight. This field is calculated using

$$\mathrm{B}_l(G) = -2.14\times10^{11}\frac{\int \mathrm{vV(v)dv}}{\lambda_0 \mathrm{gc}\int[\mathrm{I_c}-\mathrm{I(v)}]\mathrm{dv}} \tag{2}$$

from Donati et al. (1997) where v is the velocity in the star's rest frame, λ_0 the central wavelength of the LSD profile in nanometres, c is the velocity of light in vacuum, $\mathrm{g_{eff}}$ is the value of the mean Landé factor of the LSD line and $\mathrm{I_c}$ is the continuum level. This is plotted in Fig. 2. Near phase 0.0 the field peaks at a value of around 200G. The value falls to a plateau between phases $0.25-0.5$ where the field is about 150 G in the other direction. Although the individual error bars are large the plot reveals the rotational modulation of the longitudinal field, as the pattern of variability just described is repeated throughout the eight rotations that were observed.

Table 1. Spectra taken at NARVAL/TBL. The dates are all in January 2009. The observing times shown indicate the beginning of the integration. Column 4 shows the maximum signal-to-noise ratio per CCD pixel. Column 5 is the rms noise level of the polarised LSD profiles.

Date	HJD 2454800+	UT (h:m:s)	S/N	σ_{LSD} [10^{-4}]	Rotation cycle
02	34.32160	19:38:17	166	2.12	0.9302
02	34.35298	20:23:28	164	2.10	0.9470
02	34.38435	21:08:39	166	2.08	0.9637
02	34.41572	21:53:50	166	2.07	0.9804
02	34.44857	22:41:08	158	2.16	0.9980
03	35.30280	19:11:19	158	2.24	1.4544
03	35.33417	19:56:30	159	2.13	1.4712
03	35.36601	20:42:21	159	2.17	1.4882
03	35.39786	21:28:13	151	2.30	1.5052
03	35.42926	22:13:25	146	2.31	1.5220
04	36.28992	18:52:52	148	2.45	1.9818
04	36.32130	19:38:04	155	2.29	1.9985
04	36.35268	20:23:16	157	2.17	2.0153
04	36.38407	21:08:28	156	2.24	2.0320
04	36.41546	21:53:40	157	2.30	2.0488
10	42.36738	20:45:05	157	2.58	5.2286
10	42.40803	21:43:38	157	2.30	5.2502
10	42.44867	22:42:09	164	2.31	5.2720
11	43.29158	18:56:02	135	2.79	5.7224
11	43.32298	19:41:16	141	2.63	5.7391
11	43.35436	20:26:27	129	2.95	5.7559
11	43.38575	21:11:39	115	3.43	5.7727
12	44.32276	19:41:03	115	3.54	6.2733
12	44.35416	20:26:17	113	3.49	6.2900
12	44.38555	21:11:29	115	3.74	6.3068
12	44.41998	22:01:04	130	2.84	6.3251
14	46.30265	19:12:20	143	2.65	7.3310
14	46.33402	19:57:30	145	2.56	7.3478
14	46.36540	20:42:42	145	2.48	7.3645
14	46.39678	21:27:54	145	2.49	7.3812
16	48.26894	18:24:01	136	2.72	8.3815
16	48.30032	19:09:13	149	2.43	8.3983
16	48.33172	19:54:26	144	2.50	8.4150
16	48.36311	20:39:38	131	2.83	8.4318
16	48.43488	22:23:00	112	3.37	8.4701
17	49.26621	18:20:13	126	3.01	8.9143
17	49.29759	19:05:25	102	4.03	8.9310
17	49.32898	19:50:37	120	3.16	8.9478
17	49.36037	20:35:49	139	2.72	8.9646
17	49.39175	21:21:01	136	2.71	8.9813

Photometric observations of V410 Tau were obtained with two different photoelectric telescopes at different locations in Crimea, Ukraine: the 0.6-m T-60 on Mt. Koshka equipped with UBV(R)c filters for the Johnson-Cousins system, and the 1.25-m AZT-11 in Nauchny equipped with the

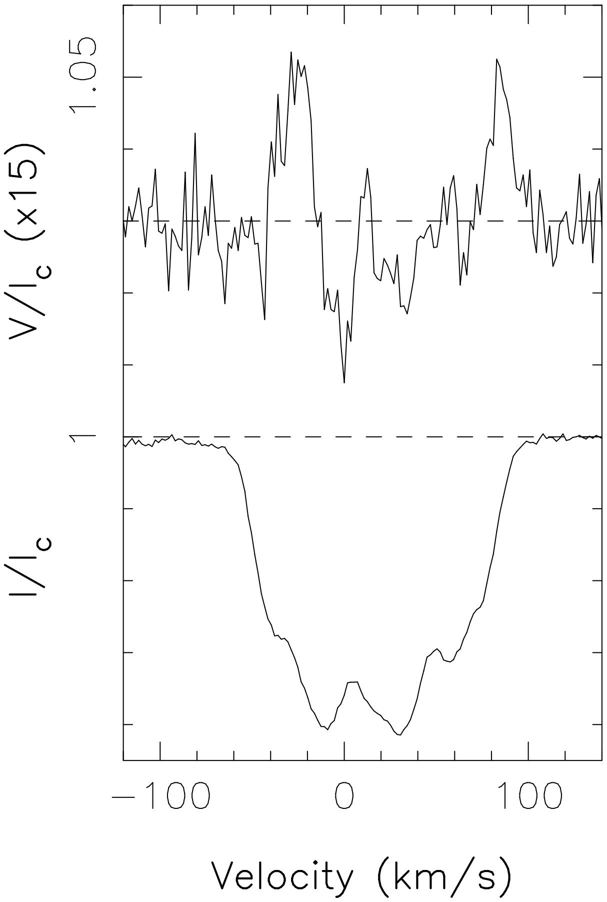

Figure 1. Example Stokes I (bottom) and V (top) profiles at phase 7.331. The V profile has been multiplied by fifteen and shifted upward by 1.03.

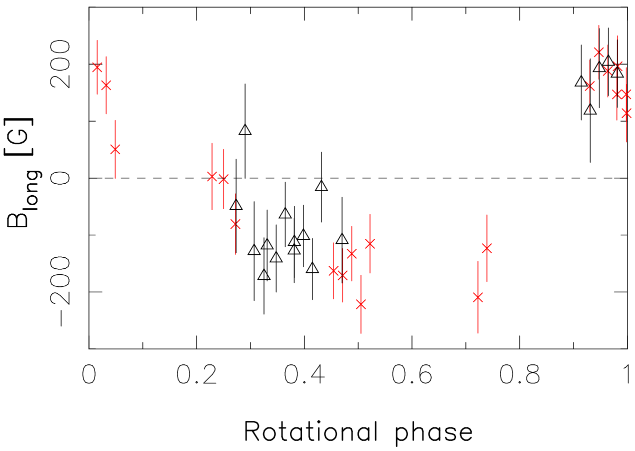

Figure 2. Line-of-sight magnetic field calculated using Eq. 2. The black triangles represent rotations $0-5$ (as listed Tab. 1) while the red crosses represent rotations $6-8$.

similar filters. Altogether, 41 UBV(R)c data points were collected for this star between 03 August 2008 and 26 January 2009. All measurements were made differentially with respect to a nearby comparison star and a check star in the the following sequence: CK-S-C-V-C-V-C-V-C-S-CK, where CK is the check star, C the comparison star, S the sky background, usually between the comparison and the variable star, and and V is the variable itself. Integration time was usually set to 10s for all filters. The data reduction was based on nightly extinction coefficients obtained from a set of standard stars. The rms error of a single measurement in the instrumental system is about 0.005 mag in BVR and 0.01 mag in U. Only the V-band lightcurve is used in this work.

4 DOPPLER AND MAGNETIC IMAGES

4.1 Zeeman-Doppler imaging process

Doppler imaging produces maps of cool photospheric spots by tracking the distortions that the spots cause to rotationally broadened spectral lines as the star rotates. Zeeman Doppler imaging extends this technique to mapping magnetic fields by applying a similar process to the circular polarisation profiles.

Details of the Zeeman Doppler imaging process have been given in several papers including Donati et al. (1997) and Donati et al. (2006). The code finds the best-fitting images using χ^2 minimisation using the I and V profiles as constraints. This cannot provide a unique solution, as the spatial resolution of the image is always limited to some extent. For this reason, entropy maximisation is used as an additional constraint, i.e. the information content of the image is minimised.

The ZDI process usually begins with a spotless star and a null magnetic field. At each step in the iteration the I and V profiles corresponding to the current image are calculated. The local line profiles are described using Gaussian profiles, which has been found to be adequate in the case of rapidly rotating stars where the shape of the local line profile is less important. The central wavelength of the mean line is 620 nm, the Landé g factor of 1.2 and a FWHM of 9.7 km s^{-1}. A linear limb-darkening law with a coefficient of 0.75 was used. The code explores the parameter space, finding stellar configuration which gives $\chi_r^2 = 1.0$ while simultaneously maximising the image entropy.

4.2 Brightness Image

The free parameters in the production of the brightness image are the spot-filling factors of each pixel of the image (Collier Cameron 1992), i.e., the fraction of each pixel which contains spot.

V410 Tau is a well-studied star, therefore the stellar parameters, including the $v \sin i$, period, radial velocity, inclination and differential rotation, have been measured in previous work (e.g., Hatzes 1995b; Rice & Strassmeier 1996; Stelzer et al. 2003). We can confirm these values using χ^2 minimisation before producing the final images. To fit the stellar parameters 1000 image pixels were used, while the final images were produced using 10000 pixels. The final reconstruction was carried out using a radial velocity of 16.8 km s^{-1}, projected rotational velocity $v \sin i = 75$ km s^{-1} and inclination $i = 70°$ (consistent with the values in the introduction). The fitting of the differential rotation and period is described in Sec. 4.4.

Fig. 3 shows the measured intensity profiles and their

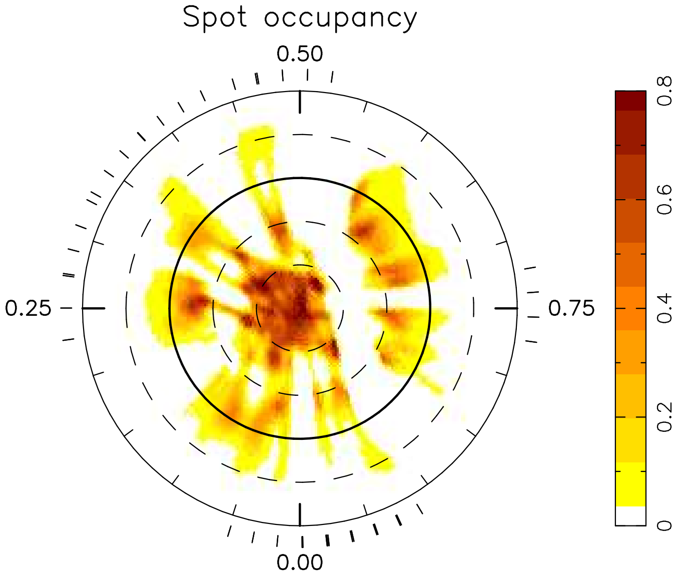

Figure 4. Doppler image of V410 Tau shown as a flattened polar projection. The colour scale represents the spot–filling factor. The circles represent lines of latitude separated by 30°, the largest circle is at latitude $-60°$ and the bold line is the equator. The numbers around the outside are rotational phases and the outer tickmarks show phases at which observations were made.

fits, while the Doppler image is shown in Fig. 4. It reveals a polar spot and groups of spots at lower latitudes. The total spot filling factor on the visible regions of the star is 8%. The lower latitude spots are concentrated in the latitude band between $0 - 30°$ and are fairly evenly spread longitudinally. The relationship between the spot distribution and the optical variability will be discussed in Sec. 5.1.

4.3 Magnetic images

The poloidal and toroidal components of the magnetic field are described using a spherical harmonic expansion with each component of the field (the radial, non-radial poloidal and toroidal field components respectively) expressed in spherical coordinates. The equations describing the field are set out in Donati et al. (2006). The advantage of using a spherical harmonic decomposition, rather than allowing each pixel to vary freely, is that the spherical harmonic description gives rise to more physically realistic solutions. For example, the code will straightforwardly return a dipole, which is unlikely when the field values in individual pixels are left as independent variables.

As the spatial resolution depends on the ratio of the width of the absorption lines to the velocity resolution in the spectra, the high $v \sin i$ of V410 Tau translates to a high resolution on the stellar surface. This allows the field to be fitted up to $l = 15$. Fig. 5 shows the resultant V profiles and the fits.

The radial, azimuthal and meridional components of the field are shown in Fig. 6. These images show a strong, apparently complicated magnetic field, with individual regions having strengths of up to 1 kG. The average field integrated over the surface of the star is 490 G. The radial component is complex with field covering a large proportion of the surface, consisting of many small regions of magnetic field and several switches in polarity. The azimuthal field covers almost the entire surface of the star, with field strengths between $300 - 1000$ G covering more than half the visible surface. There is a monolithic region of positive polarity completely covering one hemisphere, with two smaller regions of negative polarity in the opposite hemisphere. The meridional field is weaker than the radial and azimuthal components and shows positive and negative regions near the pole.

We can quantify the complexity of the field by calculating the fractional strengths of different components. The field is evenly split between the poloidal (49.2%) and toroidal (50.8%) components. The poloidal is dominated by the dipolar component, accounting for 60% of the total field. The poloidal field is nearly completely non-axisymmetric, with 5.3% of the poloidal field being axisymmetric. The implications of the magnetic topology in relation to the fields in young stars in general will be discussed in Sec. 5.2.

4.4 Differential Rotation

We carried out a measurement of differential rotation on V410 Tau by repeating the image production process described above, while incorporating a solar differential rotation law of the form

$$\Omega(\theta) = \Omega_{\rm eq} - \Delta\Omega \sin^2\theta, \tag{3}$$

where $\Omega(\theta)$ is the angular velocity as a function of latitude (θ), $\Omega_{\rm eq}$ is the angular velocity at the equator and $\Delta\Omega$ is the difference between the angular velocities at the equator and the poles.

To constrain the values of $\Omega_{\rm eq}$ and $\Delta\Omega$, we varied their values while holding the information content of the images constant, and produced a 2D plot of χ^2_r. For the Stokes I profiles the percentage spot coverage was fixed and for the Stokes V profiles the the magnetic field strength ($\rm B_{aim}$) was held constant. When the I profiles were used we were unable recover the differential rotation parameters. The difficulty here arises because the spot distribution is essentially a polar spot and a band of lower latitude spots between $0-30°$, minimising the differences between the resultant images when differential rotation parameters are introduced.

However when the V profiles alone were used in the minimisation it was possible to fit a paraboloid to the χ^2 plot. The minimum of this paraboloid identifies the $\Omega_{\rm eq}$ and $\Delta\Omega$ favoured by the data. When the code was allowed to converge with a fixed field of 400 G we obtained the χ^2 surface shown in Fig. 7. The minimum of the paraboloid fitted to this surface lies at $\Omega_{\rm eq} = 3.357 \pm 0.001$ rad day^{-1} and $\Delta\Omega = -0.007 \pm 0.006$ rad day^{-1}. This is compatible with solid body rotation as photospheric shear is less than 30% the solar value at the 3-sigma level. When different values of $\rm B_{aim}$ are used we recover very similar values of $\Omega_{\rm eq}$, $\Delta\Omega$, and their uncertainties.

4.5 Balmer Line Analysis

The Balmer line emission provides another probe of the surface activity of TTS. The Hα profile in wTTS is considered to be a superposition of a photospheric absorption component and a emission component originating in the

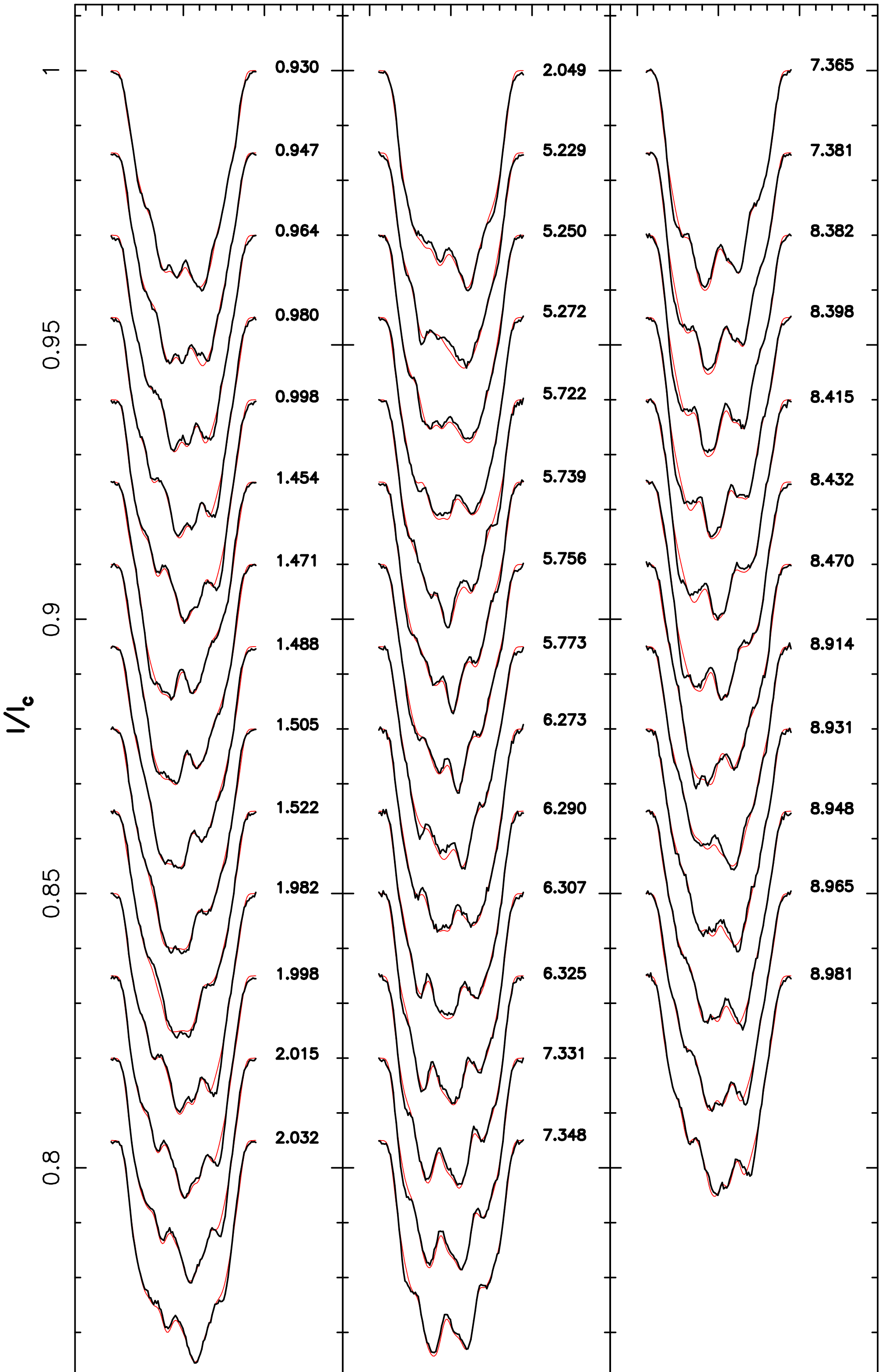

Figure 3. The I profiles produced using LSD are plotted in black and the fits are plotted with a thin red line. The number of rotational profiles completed since the ephemeris is given on the right.

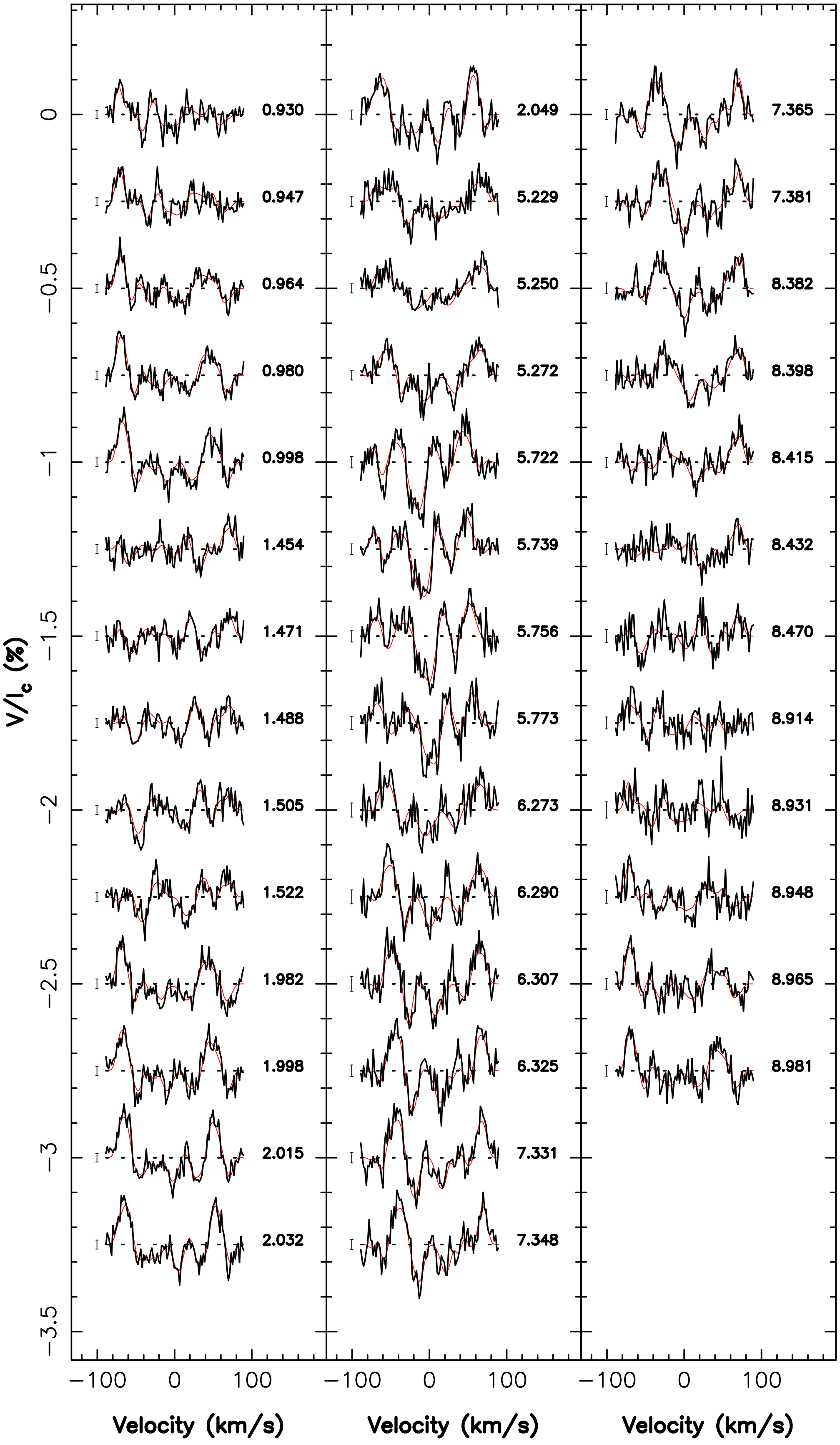

Figure 5. As Fig. 3 for V profiles. The number of rotational profiles completed since the ephemeris is given on the right. The 1-sigma error bars are on the left–hand side of each profile.

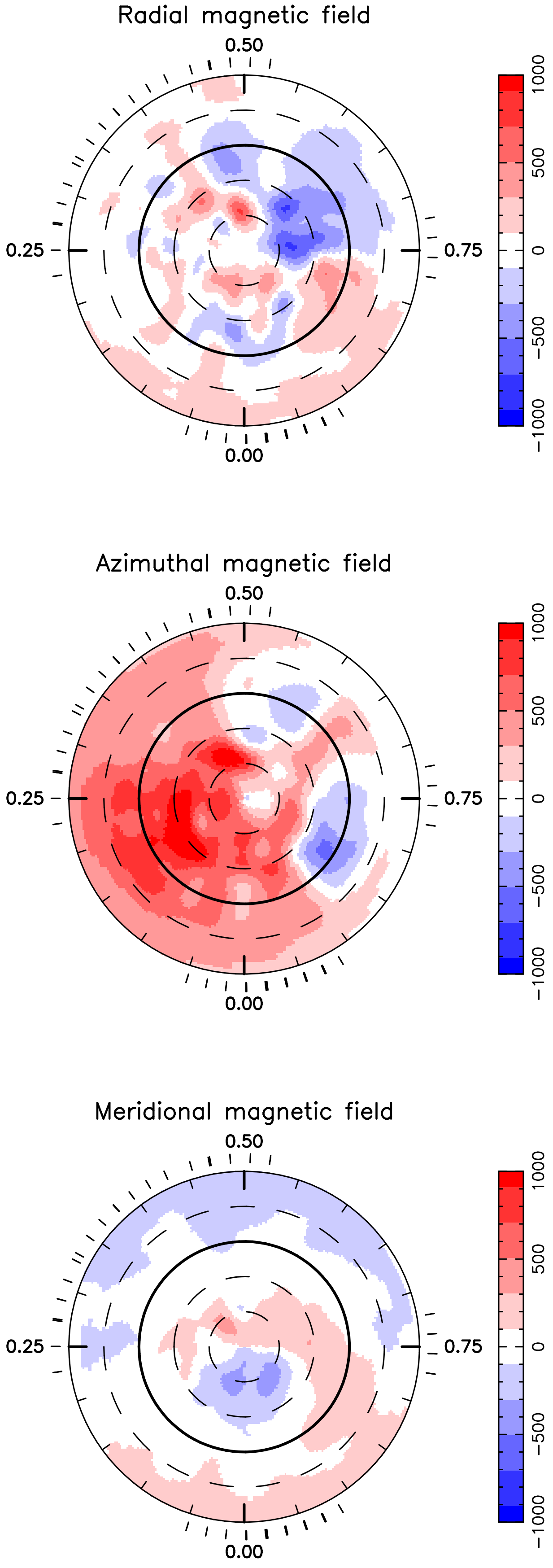

Figure 6. The magnetic images of V410 Tau, displayed using the same projection as Fig. 4. The colour scale represents the magnetic field in units of Gauss.

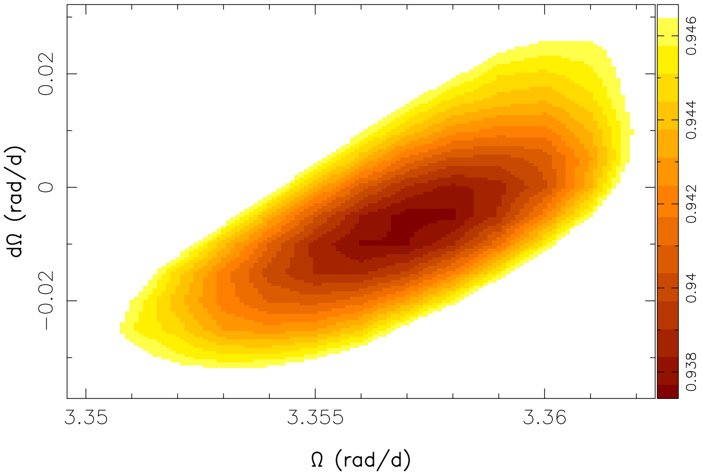

Figure 7. Reduced χ^2 surface used to deduce values of the period and differential rotation.

chromosphere and corona (cTTS have additional contributions from the disc and jet), see e.g Kurosawa et al. (2006); Barrado y Navascués & Martín (2003). The Hα profiles in V410 Tau, taken from the spectra listed in Tab. 1, show considerable variability, with the line appearing in both absorption and emission. Example profiles showing this variation are given in Fig. 8, one showing the line appearing in emission, the other when it is in absorption. In order to highlight the phase-dependence of the variability Fig. 9 shows the dynamic spectrum. This is created by stacking the profiles in order of phase and displaying as a colour plot.

The dynamic spectrum shows emission and absorption features. Hα is most strongly in emission in the phase range 0.1–0.5, suggesting the presence of chromospheric active regions (Mekkaden et al. 2005) on that hemisphere. These active regions may be connected to the large region of azimuthal field on that hemisphere (see Fig. 6).

This emission feature is crossed by an absorption transient that is centred around phase 0.4. There is a similar absorption transient between phases 0.9–1.05. When such absorption transients have been observed in other stars they have been identified with prominences crossing the stellar disc (Collier Cameron & Robinson 1989; Dunstone et al. 2006). The absorption transients appear to be passing through the spectral line more quickly than the spots (i.e. their slopes in Fig. 9 are low), suggesting that they are not very close to the surface. Calculating the variance profile (Johns & Basri 1995) reveals a symmetrical profile (not shown), with a full-width half-maximum (FWHM) of 130 km s^{-1}, and shows variance out to ±100 km s^{-1}.

The small amount of variability at velocities larger than $v \sin i$ appears to suggest that a large fraction of the variability is due to chromospheric activity. While this has been observed previously (Fernández et al. 2004), we currently favour higher-lying features due to the flat slopes of the absorption transients in Fig. 9. The absorption feature between phases 0.90 and 1.05 was observed throughout the observation run, i.e. for 8 stellar rotations, suggesting the presence of a stable feature in corotation with the star, such as a prominence. If this is the case we can estimate the height of the prominences from the slopes of the features in Fig. 9. The absorption transients cross the stel-

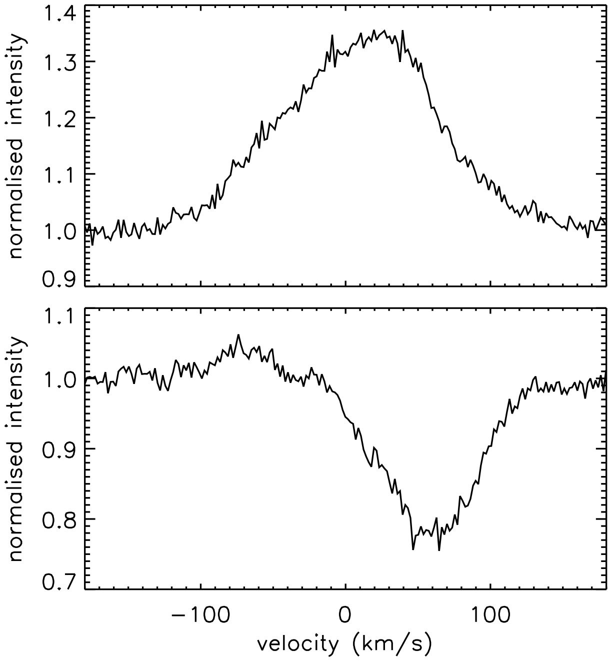

Figure 8. Example Hα profiles, showing the line in emission at phases 1.522 (top) and in absorption at phase 0.998 (bottom).

lar disc in roughly 0.15 of a rotation. Assuming the prominences are in co-rotation with the star this corresponds to a distance of 2.5 $R_*\cos\theta$ from the rotation axis, where θ is the stellar latitude. The co-rotation radius is 2.4 R_*, suggesting they may lie above co-rotation. The equations in Jardine & van Ballegooijen (2005) allow stable prominences up to a height of 7.4 R_*.

5 DISCUSSION

5.1 Optical Variability of V410 Tau

At the present time V410 Tau is displaying a low amplitude optical lightcurve, which we can attempt to relate to the image in Fig. 4. Previous images (Joncour et al. 1994; Hatzes 1995a; Rice & Strassmeier 1996; Schmidt et al. 2005) showed decentred polar spots and low latitude spots confined to particular longitude ranges. In Fig. 4 the centre of the high latitude spot is very close to the pole and the lower latitude spots are found at all longitudes, leading to less variability as the star rotates.

This variability can be quantified more precisely by comparing with the photometric data and calculating the flux differences that result from the spot distribution in Fig. 4. The photometric measurements in the V–band made at the Crimean Observatory and described in Sec. 3 are shown in Fig. 10. A synthetic lightcurve has been overplotted. This was produced by integrating the flux over the visible surface of the star at each phase. The spot–filling factors were converted to temperatures, using $T_{\rm phot} - T_{\rm spot} =$ 1400 K (Petrov et al. 1994), and then into fluxes, which are then averaged over the visible surface of the star at each phase (taking limb-darkening into account) and finally converted to a ΔV. This gives a smoothly varying function with a peak brightness at phase 0.85 and a minimum at phase 0.25. The peak-to-peak amplitude of this curve is 0.038 which is roughly consistent with the photometric measurements.

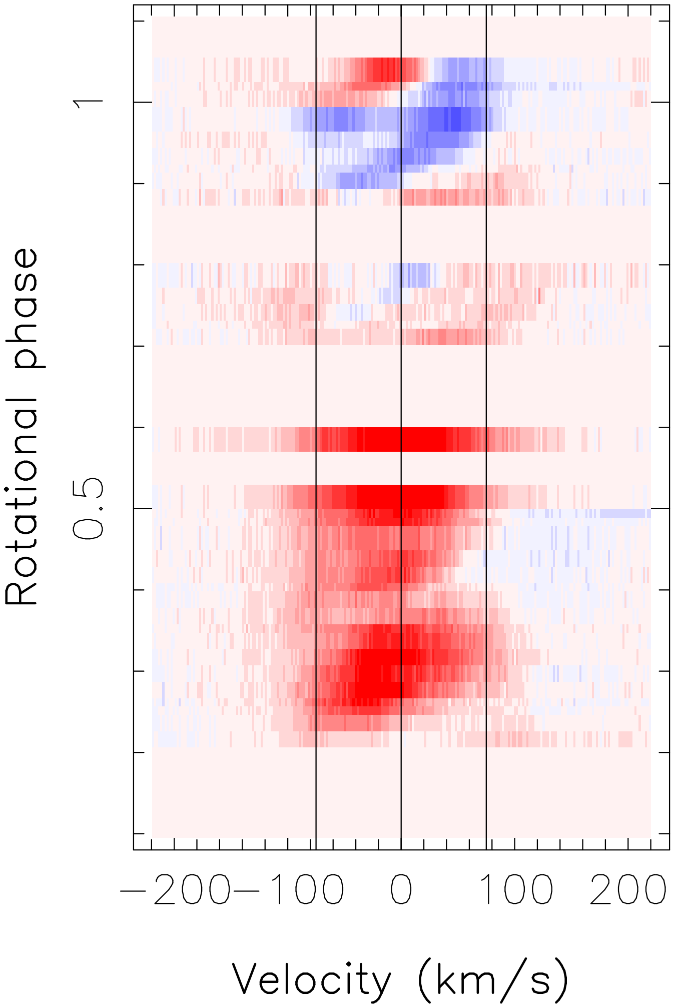

Figure 9. Dynamic spectrum of the Hα profiles. Red represents emission and blue is absorption and the normalised intensity range is between 0.7 and 1.3. The vertical lines mark the position of the $v \sin i$ (75 km s^{-1}). The phase range on the vertical axis is between 0.1–1.1 to better display the continuation of the absorption feature around phase 1.0.

We believe that the outlying point at phase is associated with a flare. The contemporaneous U–B and B–V colours provide additional evidence for this event. Discounting this point, the dispersion in the measured data points at this time is about 0.02. The mean V magnitude measured during this epoch (10.85) is similar to that measured in Grankin et al. (2008) where <V> lies between 10.8 and 10.95, further supporting the assertion that the change in the lightcurve is associated with a rearrangement in the spots.

5.2 Magnetic Nature of V410 Tau

Zeeman Doppler images have previously been created for four other TTS, all of which are cTTS. These are

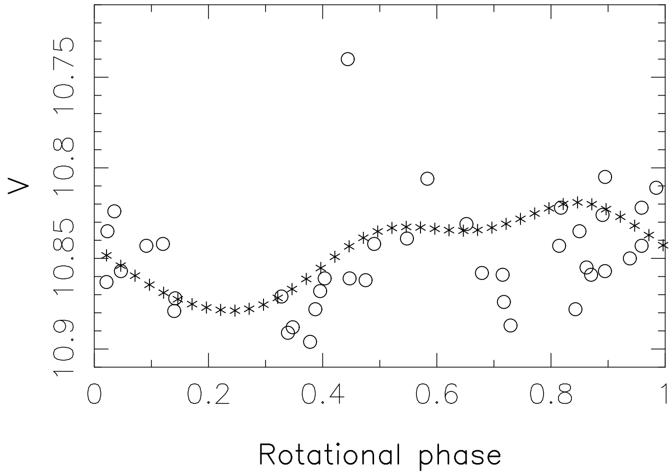

Figure 10. V magnitude as a function of rotational phase. The circles show data taken at the Crimean Observatory. The asterisks show the lightcurve calculated by integrating the flux at each phase from the image shown in Fig. 4. The latter has been shifted to have the same mean V magnitude as the photometric measurements.

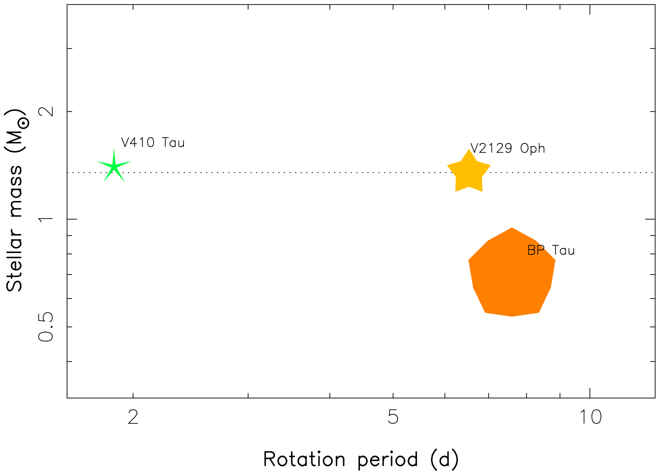

Figure 11. Plot of the mass of TTS against rotational period. The size, colour and shape of symbols represent the field strength, configuration and axisymmetry of the fields respectively. Larger symbols indicate a larger field, red stands for 100% poloidal and blue stands for 100% poloidal. A sharp five-pointed star represents a completely non-axisymmetric poloidal field and a decagon represents a completely axisymmetric poloidal field. The dotted line shows the approximate position of the fully convective limit for a 1 Myr star using the Siess et al. (2000) models.

BP Tau (Donati et al. 2008), V2129 Oph (Donati et al. 2007), CR Cha and CV Cha (Hussain et al. 2009). There is a trend observed in M dwarfs, that fully convective stars have large proportions of their fields concentrated in the lowest l and m modes and stars with radiative cores have more power concentrated in the higher l and m modes (Morin et al. 2008; Donati et al. 2008). BP Tau is a fully convective cTTS with a field which is strongly axisymmetric and dipolar, similar to fully convective main sequence stars. V2129 Oph, which has a radiative core, is dominated by an octupolar component which is approximately three times larger than the dipole. CR Cha and CV Cha are also partially convective and have significant power in higher l and m modes. The field of V410 Tau has a strong dipolar component, in common with fully convective stars, despite the fact that it appears to be partially convective (see Sec. 2). The large fraction of the field confined into the dipolar modes is significant, given that the high $v \sin i$ of V410 Tau means that we are sensitive to the higher orders in the spherical harmonic decomposition.

Fig. 11 compares the magnetic topology of V410 Tau with BP Tau and V2129 Oph, using the conventions in Donati et al. (2008) and Morin et al. (2008), who investigated the magnetic topology of M dwarfs. While we cannot infer trends from this plot from only three data points it allows direct comparison between these TTS. V2129 Oph and V410 Tau have similar physical structures, with closely matched masses and similar radiative core sizes (~ 0.2 R$_*$ for V2129 Oph). However, there are significant differences between the fields of the two stars. The field of V410 Tau is more strongly poloidal, and is much less axisymmetric. It is rotating more rapidly than the cTTS BP Tau and V2129 Oph (due to the absence of disk-braking), but this does not lead to commensurately larger fields as it is the fully convective BP Tau which generates the largest magnetic field, despite its lower rotation rate. It appears that the depth of the convection zone plays a role in determining the field strength, although we do appear to observe the sharp transition in field topology that is seen in M dwarfs. We anticipate adding more stars as the data on TTS become available.

Qualitatively, the field of V410 Tau most resembles older, rapidly rotating stars such as AB Dor (Donati & Collier Cameron 1997; Donati et al. 1999, 2003b; Hussain et al. 2007), rather than the classical TTS discussed above. AB Dor is a 50 Myr old (i.e. post-T Tauri) K0 star with a $v \sin i$ of 90 km s^{-1}. The similarities between the magnetic maps of the two stars are monolithic regions of azimuthal field, almost forming rings around the pole and complex radial fields with many switches in polarity.

AB Dor and V410 Tau are broadly similar in the sense that they are young and rapidly rotating. However V410 Tau has almost solid body rotation while AB Dor has significant differential rotation, with $\Delta\Omega$ (see Eq. 3) having values between 0.043 – 0.074 rad day^{-1} (Collier Cameron & Donati 2002; Donati et al. 2003,a; Jeffers et al. 2007).

Usually, strong azimuthal field is associated with differential rotation. For instance an $\alpha\Omega$ dynamo gives rise to toroidal field through differential rotation shearing the poloidal field. The field topology of V410 Tau is therefore somewhat difficult to understand.

While the qualitative similarity of the field with those of partially–convective stars such as AB Dor suggests that V410 Tau has a radiative core, we cannot rule out the possibility that V410 Tau is fully convective, as Sec. 2 suggested. In this case the dipolar component of the field follows the trend observed in other TTS and M dwarfs. However, the question of the origin of the azimuthal component remains, due to the lack of observed differential rotation.

Further magnetic and brightness maps will follow from this campaign on V410 Tau. We also have spectra of several other TTS which will be used to produce magnetic images.

Using these data, we expect to gain a better insight into the form and evolution of dynamos in pre-main sequence stars.

6 CONCLUSIONS

The Doppler image of the weak-line T Tauri star V410 Tau in January 2009 shows a large polar spot and a several lower latitude spots spread around the latitude band between $0 - 30°$. This spot distribution can explain the relatively flat V–band lightcurve currently being observed on the star as, unlike during previous Doppler imaging campaigns, the spots are not confined to a particular longitude range. The polar spot on the image is centred on the pole, unlike on previous images where it was shifted from the pole.

The Hα profile is complex and highly variable. Fast-moving absorption transients in the line may indicate the presence of high-lying circumstellar material, such as sling-shot prominences.

The magnetic field is predominately dipolar and non-axisymmetric. It has a complex radial field as well as a strong azimuthal field with large monolithic regions. The field resembles zero-age main sequence stars such as AB Dor, but unlike that star it has very weak differential rotation. The rotation rate and depth of convection zone appear to be the most important parameters in determining the strength and configuration of the magnetic field

Future Zeeman Doppler images planned as part of a campaign on Télescope Bernard Lyot (TBL) will reveal whether changes in the amplitude of the optical lightcurve are accompanied by significant changes in the spot distribution or magnetic field topology.

ACKNOWLEDGMENTS

We thank the TBL staff for their help during data collection and the anonymous referee for constructive comments that have improved the clarity of the text. This work was supported by the French “Agence Nationale pour la Recherche” (ANR) within the “Magnetic Protostars and Planets” (MaPP) project.

REFERENCES

Barnes J. R., 2005, Mon. Not. R. Astron. Soc. , 364, 137

Barnes J. R., Cameron A. C., Donati J.-F., James D. J., Marsden S. C., Petit P., 2005, Mon. Not. R. Astron. Soc. , 357, L1

Barnes J. R., Collier Cameron A., James D. J., Donati J.-F., 2001, Mon. Not. R. Astron. Soc. , 324, 231

Barrado y Navascués D., Martín E. L., 2003, Astron. J. , 126, 2997

Berdyugina S. V., 2005, Living Reviews in Solar Physics, 2, 8

Bertout C., Robichon N., Arenou F., 1999, Astron. Astrophys. , 352, 574

Bertout C., Siess L., Cabrit S., 2007, Astron. Astrophys. , 473, L21

Bessell M. S., Castelli F., Plez B., 1998, Astron. Astrophys. , 333, 231

Collier Cameron A., 1992, LNP Vol. 397: Surface Inhomogeneities on Late-Type Stars, 397, 33

Collier Cameron A., Donati J.-F., 2002, Mon. Not. R. Astron. Soc. , 329, L23

Collier Cameron A., Robinson R. D., 1989, Mon. Not. R. Astron. Soc. , 236, 57

Donati J.-F., Cameron A. C., Semel M., Hussain G. A. J., Petit P., Carter B. D., Marsden S. C., Mengel M., López Ariste A., Jeffers S. V., Rees D. E., 2003a, Mon. Not. R. Astron. Soc. , 345, 1145

Donati J.-F., Cameron A. C., Semel M., Hussain G. A. J., Petit P., Carter B. D., Marsden S. C., Mengel M., López Ariste A., Jeffers S. V., Rees D. E., 2003b, Mon. Not. R. Astron. Soc. , 345, 1145

Donati J.-F., Collier Cameron A., 1997, Mon. Not. R. Astron. Soc. , 291, 1

Donati J.-F., Collier Cameron A., Hussain G. A. J., Semel M., 1999, Mon. Not. R. Astron. Soc. , 302, 437

Donati J.-F., Collier Cameron A., Petit P., 2003, Mon. Not. R. Astron. Soc. , 345, 1187

Donati J.-F., Howarth I. D., Jardine M. M., Petit P., Catala C., Landstreet J. D., Bouret J.-C., Alecian E., Barnes J. R., Forveille T., Paletou F., Manset N., 2006, Mon. Not. R. Astron. Soc. , 370, 629

Donati J.-F., Jardine M. M., Gregory S. G., Petit P., Bouvier J., Dougados C., Ménard F., Cameron A. C., Harries T. J., Jeffers S. V., Paletou F., 2007, Mon. Not. R. Astron. Soc. , 380, 1297

Donati J.-F., Jardine M. M., Gregory S. G., Petit P., Paletou F., Bouvier J., Dougados C., Ménard F., Cameron A. C., Harries T. J., Hussain G. A. J., Unruh Y., Morin J., Marsden S. C., Manset N., Aurière M., Catala C., Alecian E., 2008, Mon. Not. R. Astron. Soc. , 386, 1234

Donati J.-F., Morin J., Petit P., Delfosse X., Forveille T., Aurière M., Cabanac R., Dintrans B., Fares R., Gastine T., Jardine M. M., Lignières F., Paletou F., Velez J. C. R., Théado S., 2008, Mon. Not. R. Astron. Soc. , 390, 545

Donati J.-F., Semel M., Carter B. D., Rees D. E., Collier Cameron A., 1997, Mon. Not. R. Astron. Soc. , 291, 658

Dunstone N. J., Barnes J. R., Cameron A. C., Jardine M., 2006, Mon. Not. R. Astron. Soc. , 365, 530

ESA 1997, VizieR Online Data Catalog, 1239, 0

Fernández M., Stelzer B., Henden A., Grankin K., Gameiro J. F., Costa V. M., Guenther E., Amado P. J., Rodriguez E., 2004, Astron. Astrophys. , 427, 263

Grankin K. N., 1999, Astronomy Letters, 25, 526

Grankin K. N., Bouvier J., Herbst W., Melnikov S. Y., 2008, Astron. Astrophys. , 479, 827

Hatzes A. P., 1995a, Astrophys. J. , 451, 784

Hatzes A. P., 1995b, Astron. J. , 109, 350

Herbst W., 1989, Astron. J. , 98, 2268

Hussain G. A. J., Collier Cameron A., Jardine M. M., Dunstone N., Ramirez Velez J., Stempels H. C., Donati J. ., Semel M., Aulanier G., Harries T., Bouvier J., Dougados C., Ferreira J., Carter B. D., Lawson W. A., 2009, ArXiv e-prints

Hussain G. A. J., Jardine M., Donati J.-F., Brickhouse N. S., Dunstone N. J., Wood K., Dupree A. K., Collier Cameron A., Favata F., 2007, Mon. Not. R. Astron. Soc. , 377, 1488

Jardine M., van Ballegooijen A. A., 2005, Mon. Not. R. Astron. Soc. , 361, 1173

Jeffers S. V., Donati J.-F., Collier Cameron A., 2007, Mon. Not. R. Astron. Soc. , 375, 567

Johns C. M., Basri G., 1995, Astrophys. J. , 449, 341

Joncour I., Bertout C., Menard F., 1994, Astron. Astrophys. , 285, L25+

Kurosawa R., Harries T. J., Symington N. H., 2006, Mon. Not. R. Astron. Soc. , 370, 580

Kurucz R. L., 1993, VizieR Online Data Catalog, 6039, 0

Mekkaden M. V., Pukalenthi S., Muneer S., Bastian A. B., 2005, Bulletin of the Astronomical Society of India, 33, 433

Morin J., Donati J.-F., Forveille T., Delfosse X., Dobler W., Petit P., Jardine M. M., Cameron A. C., Albert L., Manset N., Dintrans B., Chabrier G., Valenti J. A., 2008, Mon. Not. R. Astron. Soc. , 384, 77

Morin J., Donati J.-F., Petit P., Delfosse X., Forveille T., Albert L., Aurière M., Cabanac R., Dintrans B., Fares R., Gastine T., Jardine M. M., Lignières F., Paletou F., Ramirez Velez J. C., Théado S., 2008, Mon. Not. R. Astron. Soc. , 390, 567

Oláh K., Kolláth Z., Granzer T., Strassmeier K. G., Lanza A. F., Järvinen S., Korhonen H., Baliunas S. L., Soon W., Messina S., Cutispoto G., 2009, Astron. Astrophys. , 501, 703

Parker E. N., 1955, Astrophys. J. , 122, 293

Petrov P. P., Shcherbakov V. A., Berdyugina S. V., Shevchenko V. S., Grankin K. N., Melnikov S. Y., 1994, Astron. Astrophys. Suppl. , 107, 9

Rice J. B., Strassmeier K. G., 1996, Astron. Astrophys. , 316, 164

Rüdiger G., Elstner D., Ossendrijver M., 2003, Astron. Astrophys. , 406, 15

Schmidt T., Guenther E., Hatzes A. P., Ries C., Hartmann M., Ohlert J. M., Lehmann H., 2005, Astronomische Nachrichten, 326, 667

Semel M., 1989, Astron. Astrophys. , 225, 456

Sestito P., Palla F., Randich S., 2008, Astron. Astrophys. , 487, 965

Siess L., Dufour E., Forestini M., 2000, Astron. Astrophys. , 358, 593

Skelly M. B., Unruh Y. C., Cameron A. C., Barnes J. R., Donati J.-F., Lawson W. A., Carter B. D., 2008, Mon. Not. R. Astron. Soc. , 385, 708

Sokoloff D. D., Nefedov S. N., Ermash A. A., Lamzin S. A., 2008, Astronomy Letters, 34, 761

Stelzer B., Fernández M., Costa V. M., Gameiro J. F., Grankin K., Henden A., Guenther E., Mohanty S., Flaccomio E., Burwitz V., Jayawardhana R., Predehl P., Durisen R. H., 2003, Astron. Astrophys. , 411, 517

Strassmeier K. G., 2002, Astronomische Nachrichten, 323, 309

Strassmeier K. G., 2009, Astronomy. Astrophys. Rev. , 17, 251

Vogt S. S., Penrod G. D., Hatzes A. P., 1987, Astrophys. J. , 321, 496

Vrba F. J., Herbst W., Booth J. F., 1988, Astron. J. , 96, 1032

Wichmann R., Bastian U., Krautter J., Jankovics I., Rucinski S. M., 1998, Mon. Not. R. Astron. Soc. , 301, L39+